Environ. Sci. Technol. **2008,** *42,* 5772–5778

Mercury Vapor Release from Broken Compact Fluorescent Lamps and In Situ Capture by New Nanomaterial Sorbents

NATALIE C. JOHNSON, SHAWN MANCHESTER, LOVE SARIN, YUMING GAO, INDREK KULAOTS, AND ROBERT H. HURT*

Division of Engineering and Institute for Molecular and Nanoscale Innovation, Brown University, Providence, Rhode Island

Received February 14, 2008. Revised manuscript received May 18, 2008. Accepted May 20, 2008.

The projected increase in the use of compact fluorescent lamps (CFLs) motivates the development of methods to manage consumer exposure to mercury and its environmental release at the end of lamp life. This work characterizes the time-resolved release of mercury vapor from broken CFLs and from underlying substrates after removal of glass fragments to simulate cleanup. In new lamps, mercury vapor is released gradually in amounts that reach 1.3 mg or 30% of the total lamp inventory after four days. Similar time profiles but smaller amounts are released from spent lamps or from underlying substrates. Nanoscale formulations of S, Se, Cu, Ni, Zn, Ag, and WS_2 are evaluated for capture of Hg vapor under these conditions and compared to conventional microscale formulations. Adsorption capacities range over 7 orders of magnitude, from 0.005 (Zn micropowder) to 188 000 μg/g (unstabilized nano-Se), depending on sorbent chemistry and particle size. Nanosynthesis offers clear advantages for most sorbent chemistries. Unstabilized nano-selenium in two forms (dry powder and impregnated cloth) was successfully used in a proof-of-principle test for the in situ, real-time suppression of Hg vapor escape following CFL fracture.

Introduction

Fluorescent lighting technologies are undergoing rapid market growth as part of a resurgent societal interest in energy efficiency. Much of current and projected growth is in the domestic use of compact fluorescent lamps (CFLs), which offer consumers approximately 75% reduction in energy usage and 10-fold increase in lifetime relative to incandescent bulbs. Federal legislation in the U.S. will phase out incandescent bulbs by 2012 and likely cause their replacement by CFLs. Fluorescent lamps contain 0.7−115 mg of Hg per lamp (*1*), and the subclass of CFLs on average contain 3−5 mg per lamp. Mercury is a well-known human toxicant that is of special concern for neural development in unborn and growing children.

While most Hg-containing products are being removed from homes and workplaces through substitution programs, CFL use is increasing sharply because the environmental benefits (reduced energy consumption and coal combustion emissions) (*2*) are widely recognized to outweigh the health risks. Indeed an individual CFL contains much less Hg than some older home devices (e.g., 500 mg for a typical older model fever thermometer), but the projected sales volumes for CFLs are large. The Association of Lighting and Mercury Recyclers report that 700 million Hg-containing lamps are discarded each year with only a 24% recycle rate. Domestic CFL sales are likely to increase these numbers significantly, and currently 98% are not recycled. There is strong motivation to improve Hg management over the life-cycle of these rapidly proliferating consumer products. Our present work is motivated by two specific issues in the management of Hg from CFLs:

1. *Direct exposure of consumers or workers to Hg vapor from fractured or crushed lamps.* Some lamps are inevitably broken accidentally during shipping, retail sales, consumer use, and recycling and release a portion of their mercury inventory as volatile Hg^0 vapor, which is the dominant mercury form in the early stages of lamp life (*3*). Inhalation exposure is a concern because 80% of inhaled Hg is physiologically absorbed (*4*). The OSHA occupational exposure limit (8 h, 5-day week time average) is 100 $\mu g/m^3$. The NIOSH recommended exposure limit is 50 $\mu g/m^3$, while American Conference of Governmental and Industrial Hygienists recommends 25 $\mu g/m^3$ under the same conditions (*4*). Because children are more susceptible, the Agency for Toxic Substances and Disease Registry (ATSDR) recommends 0.2 $\mu g/m^3$ level as a safe continual exposure limit for children (*4*). As an illustration of the effects of CFL breakage, the release of only 1 mg of Hg vapor (~20% of the Hg inventory in a single CFL) into a 500 m^3 room (10 × 10 × 5m) yields 2.0 $\mu g/m^3$ or ten times the ATSDR-recommended level of 0.2 $\mu g/m^3$ in the absence of ventilation.There is limited information on the timing and extent of Hg vapor release from fractured lamps (*1, 2, 5*), especially the new CFLs. Jang et al. (*1*) report only 0.04−0.17% of the Hg as vapor, but this was a study of the phase partitioning *within the bulb volume*, not a study of the gradual evaporation and release characteristics upon fracture under atmospheric conditions, where we find much larger amounts of Hg vapor (see below). Following any mercury spill, hard surfaces can be cleaned, but in the absence of in situ treatment technologies, porous materials such as carpets or woodwork must be removed and discarded (*4*). Carpet vacuuming can release Hg vapor when large gas volumes are forced across the Hg-containing dust cake in the vacuum cleaner internal filter. If not removed, spilled Hg liquid will continue to release vapor over time and can spread to other sites through foot traffic. Most consumer information on CFLs claim there is no significant health risk from small numbers of broken lamps, and indeed, since the 1960s, examples of Hg poisoning from all sources have become rare (*6*). There is one report of Hg poisoning (acrodynia) in a child exposed to broken tube-type fluorescents in a detailed case study presented by Tunnessen et al. (*6*). Overall, there is significant motivation to improve our management of Hg exposures caused by accidental breakage of fluorescent lamps.

2. *Release of Hg to the environment at end of lamp life.* The main route of human exposure to mercury is through environmental release followed by bacterial methylation, bioaccumulation in aquatic food webs, and fish consumption (*7*). Methyl-Hg is listed by the International Program of Chemical Safety as one of the most dangerous chemicals in the environment (*8, 9*), and one in twelve women of childbearing age are reported to have blood mercury levels above the EPA reference dose (*10*). Methyl-Hg not only crosses

* Corresponding author e-mail: Robert_Hurt@brown.edu.

10.1021/es8004392 CCC: $40.75
Published on Web 06/27/2008

the human placenta but also accumulates at higher concentrations on the fetal side than on the maternal and crosses the blood-brain barrier, where it is retained (*9, 11*). Currently 98% of CFLs are not recycled, and there is concern about Hg leaching from landfills. The EPA has concluded that mercury can be present in significant concentrations in the leachate and groundwater at nonhazardous landfill sites and can migrate offsite to threaten drinking water supplies (*2*). Mercury in new lamps is primarily in elemental form, but over time interacts with the phosphor and glass to produce a more complex internal partitioning in spent lamps, which contain elemental, immobile (glass matrix imbedded), and oxidized soluble forms (*3, 5, 12*). Landfill leaching can be minimized by avoiding or reducing the mercury to water-soluble oxidized forms. Some manufacturers are reported to incorporate reducing agents in lamps to improve performance in TCLP testing. This approach may protect local groundwater but would lead to formation of volatile elemental mercury and enhanced environmental release of the vapor in landfill gases. The largest source of anthropogenic mercury emission is now coal-fired power plants (48 ton/year), which is much larger than even the total annual inventory of spent lamps (700 million × 8 mg = approximately 5.6 tons). New regulations on power plant emissions, however, should reduce coal-derived Hg by 70% to 15 tons/year by 2018 (*13*), which coupled with rapid projected growth in CFLs may make lamp-derived mercury a more significant fraction of the total environmental burden.

Common to both issues (direct exposure and environmental release) is the motivation to develop better methods for Hg vapor capture and stabilization at ambient temperatures. High-efficiency, low-temperature Hg sorbents could be used in reactive barrier cloths to remediate carpets and porous substrates after CFL breakage or incorporated into disposal bags or modified retail package materials as receptacles for spent lamps to prevent end-of-life release. The goal of the present work is therefore 2-fold: (i) to characterize the release of Hg vapor from CFLs as a function of time since fracture and (ii) to identify and evaluate new high-efficiency sorbents for ambient temperature capture focusing on new methods of nanosynthesis.

Materials and Methods

Compact Fluorescent Lamps and Hg Release Characteristics. Two different brands of compact fluorescent lamps were purchased commercially: 13 and 9 W devices containing 4.5 and 5.0 mg of mercury respectively. Used bulbs were collected from local residences and retail recycling centers. To characterize the release of Hg vapor under ambient conditions, the bulbs were catastrophically fractured inside a flexible Teflon enclosure (volume 2 L) and the Hg vapor transported away by a metered flow of nitrogen (1 LPM). A portion of the Hg-contaminated flow was passed to a gold amalgamation atomic fluorescent vapor-phase mercury analyzer (PSA model 10.525), and the concentration-time profiles were measured and integrated to obtain total sorbent capacity for mercury.

The effectiveness of several sorbents in capturing mercury released from fractured CFLs was tested in a proof-of-principle experiment using the flow system discussed above. The CFL was again fractured in the flexible 2 L Teflon enclosure, which also contained sorbent as loose powder or impregnated cloth. After lamp fracture, the enclosure was isolated from the flow system for 24 h. At the end of this period, the enclosure was reintegrated into the flow system, the high purity nitrogen stream was initiated, and the effluent was analyzed for mercury content.

Sorbents and Mercury Adsorption Capacity Measurements. A variety of carbon materials were used in this study (see Table 1) including Darco FGL activated carbon, Alfa Aeser granulated activated carbon, Cabot M-120 carbon black, sulfur impregnated carbon sample (HgR), and a mesoporous carbon (*14*). The origin, particle sizes, and surface areas of commercial sulfur used in this work are provided in Table 1, which also gives the mercury capture capacity of the sorbents in our standard gas environment (60 μg Hg/m^3 argon at 20 C as described below). Sulfur nanotubes were synthesized at Brown by immersion of 200 nanometer channel aluminum templates in a 50 mass % solution of Sigma Aldrich 100 mesh commercial sulfur in CS_2. The loaded templates were dried, and excess sulfur was removed from the template top with a razor blade. The aluminum templates were etched overnight with 2 M NaOH solution. The S-nanotube samples were washed twice with 1 M NaOH, twice with 0.5 M NaOH and four times with DI water, followed by centrifugation and oven drying at 60 °C. See Table 1 and for the source, particle sizes, and surface areas of the metals and metal sulfides used as sorbents in this study.

Amorphous nano-selenium was prepared using a 4:1 molar mixture of glutathione (GSH, reduced form, TCI America) and sodium selenite (Na_2SeO_3, Alfa Aesar) solution. Glutathione reduces sodium selenite to form seleno-diglutathione (GSSeSG), which decomposes to elemental selenium as upon sodium hydroxide titration (*15, 16*). In the presence of bovine serum albumin (BSA, Sigma-Aldrich), the reaction gives a stabilized nano-selenium dispersion (*17*). For mercury capture experiments, the solutions of nano-selenium were divided in 1.5−2 mL aliquots and freeze-dried to prevent any thermal effects of heat drying. The nano-selenium samples were pelletized by centrifugation (13 000 rpm, 10 min) before freeze-drying. These freeze-dried aliquots and Se-impregnated cloth, which was prepared by soaking a 15 × 17 in. Kimwipe in the amorphous nano-selenium solution and drying at room temperature, were used for the in situ mercury release experiments. A commercial selenium sample was obtained in the form of pellets (J.T. Baker) and crushed to obtain Se powder of 2−200 μm. Manchester et al. (*18*) and the Supporting Information provide more detailed description of Hg adsorption capacity measurement and analysis.

Results and Discussion

Mercury Release Characteristics from Broken CFLs. Figure 1 shows time-resolved mercury release data from two CFL models. The release is initially rapid producing vapor concentrations from 200−800 μg/m^3 during the first hour, which far exceed the OSHA occupational limits. The release decays on a time scale of hours and continues at significant rate for at least four days (data beyond 24 h not shown). The total Hg released after 24 h is 504 (13 W model) and 113 μg (for 9 W) by integration, which are 11.1% and 1.9% of the total Hg content specified by the vendors, respectively. Over 4 days (extended data not shown), the 13 W bulb released 1.34 mg or 30% of the total Hg. In general, Hg° evaporation is known to be slow under ambient conditions, and our data suggest that much of the original mercury remains in the bulb debris after 96 h and will continue to evaporate slowly. Saturated Hg° vapor (15 000 μg/m^3) in a typical lamp volume (50 mL) corresponds to only 0.65 μg of vapor phase Hg°, which is much less than the actual mercury release during the first hour, 12−43 μg. The majority of Hg in a CFL must therefore be in a condensed phase originally, and the mercury release we observe must be primarily caused by desorption/evaporation phenomena. Figure 1 also compares the actual CFL release with the evaporation of a free Hg° droplet under the same set of conditions. The actual CFL release exceeds the release from a free Hg° droplet of equal mass (see Figure 1), which likely reflects the much larger surface area of the adsorbed phase (on the phosphor, end caps, or glass) relative to the single drop. Similar release patterns but lower amounts

TABLE 1. Comparative Summary of Low-Temperature Mercury Vapor Sorbents

sorbent description	surface area (particle size)	Hg capture capacity (μg/g)[a]
sulfur		
micro-sulfur (Sigma Aldrich)	0.3 m^2/g (~10 μm)	0.026
sulfur nanotubes	30 m^2/g (~200 nm)	0.62
metals and metal oxides		
micro-zinc (Sigma Aldrich)	0.2 m^2/g (4.2 μm)	0.005
nano-zinc (Sigma Aldrich)	3.7 m^2/g (230 nm)	0.08
micro-nickel (Sigma Aldrich)	0.5 m^2/g (1.5 μm)	0.04
nano-nickel (Alfa Aesar)	15.9 m^2/g (43 nm)	1.5
micro-copper (Sigma Aldrich)	0.4 m^2/g (1.7 μm)	2.5
nano-copper (Alfa Aesar)	13.5 m^2/g (50 nm)	31.8
aged nano-copper	see nano-Cu	71.3
nano-copper-oxide	see nano-Cu	4.3
nano-silver (Inframat Advanced Materials)	(50−100 nm by TEM)	8510
nano-silver, 500°C vacuum annealed	(100−500 nm)	2280
metal sulfides		
micro-MoS_2 (Sigma-Aldrich)	(<2 μm)	7
micro-WS_2 (Sigma-Aldrich)	(<2 μm)	25
nano-WS_2 (Nanostructured & Amorphous Materials Inc.)	30 m^2/g (100−500 nm)[b]	27
carbon		
carbon black (Cabot M120)	38 m^2/g (75 nm)	0.45
mesoporous carbon (Jian et al.) (*14*)	144 m^2/g (24 nm pore size)	1.25
activated carbon 1, undoped[c]	900 m^2/g[b]	20
activated carbon 2, undoped[c]	550 m^2/g[b]	115
activated carbon 3, S-impregnated (HgR, Calgon Carbon Corp.)	1000−1100 m^2/g[b]	2600
selenium		
micro-Se (commercial, ground, amorphous)	0.03 m^2/g (10−200 μm)	>5000
BSA-stabilized amorph. nano-Se	65 m^2/g (6−59 nm)	616
BSA (alone) [d]		6.3
glutathione, GSH (alone) [d]		1.3
glutathione, oxidized, (alone) [d]		0.3
unstabilized amorph. nano-Se	9 m^2/g (12−615 nm)	188 000
commercial products for Hg vapor capture		
product 1	(10−200 μm)	7
product 2	(10−200 μm)	1250

[a] Inlet gas stream at 20 °C, 60 μg/m^3 Hg. [b] Data provided by manufacturer. [c] Manchester et al. (*18*). [d] Byproducts of nanoselenium synthesis.

were seen for spent bulbs (example result 90 μg in 24 h) or from the fracture site of a new bulb after glass removal to simulate cleanup. Removing large glass shards by hand after breakage on a carpet did not eliminate Hg release, but reduced it by 67% relative to the data in Figure 1. The remaining (33%) release from the fracture site is believed to be primarily associated with spilled phosphor powder, which is known to be the primary site for adsorbed Hg partitioning in fresh bulbs (*1*).

Sorbent Synthesis, Characterization, and Testing. Because mercury vapor capture on solids occurs by adsorption or gas−solid reaction where kinetics or capacities typically depend on surface area (in addition to other factors such as composition), we hypothesized that high-area, nanoscale formulations of common mercury sorbents will show enhanced performance. This section evaluates a large set of new nanomaterial sorbents for ambient temperature Hg^0 vapor capture and compares their performance to conventional microscale formulations of the same materials. Manchester et al. (*18*) shows an example breakthrough curve that is the raw output of the fixed-bed sorbent tests. Integrating the area between the baseline inlet (60 μg/m^3) and the outlet concentration curve and dividing by sorbent mass yields a capacity reported in μg-Hg/g-sorbent (*18*). Table 1 is a complete list of the sorbents and their Hg capacities under our standard conditions (60 μg/m^3 inlet stream), and the following sections discuss the results by sorbent class.

Sulfur. Sulfur-containing materials are widely used for mercury capture (*19, 20*). Zero-valent sulfur reacts with mercury to form stable mercuric sulfide in one of two crystal forms: red cinnabar ($\Delta H_f^\circ = -58$ kJ/mol, $\Delta G_f^\circ = -49$ kJ/mol) or black metacinnabar ($\Delta H_f^\circ = -54$ kJ/mol, $\Delta G_f^\circ = -46$ kJ/mol) and is thus attractive for waste or stockpile stabilization (*20, 21*). Oji (*20*) discusses the advantages of HgS relative to Zn amalgam for the stabilization and disposal of Hg-containing mixed wastes, and Svensson et al. (*21*) discuss favorable conditions for HgS formation from Hg or HgO in geological repositories. Surprisingly, there are few reports of nano-sulfur synthesis (*22–24*) and to our knowledge no studies of nano-sulfur as a mercury sorbent.

Here we choose a convenient templating route to obtain small quantities of nanostructured sulfur for sorbent testing. Figure 2 shows the morphology and sorption behavior of sulfur nanotubes fabricated by spontaneous infiltration of CS_2/S solutions into nanochannel alumina templates followed by solvent evaporation and chemical etching of the template. The sulfur nanotubes show a 90-fold increase in surface area and a 24-fold increase in Hg capacity over conventional powdered sulfur. The total captured Hg is much less than the HgS stoichiometric limit and much less than even surface monolayer capacity, and the capacities increase with increasing temperature. These results indicate a kinetically limited chemisorption/reaction on active sites that represent a small fraction of the nanotube surfaces.

Metals and Metal Sulfides. There is an extensive literature on Hg interaction with metals (*25–28*), much of it focused on elevated temperatures using conventional film or microparticle formulations. Here we investigate newly available

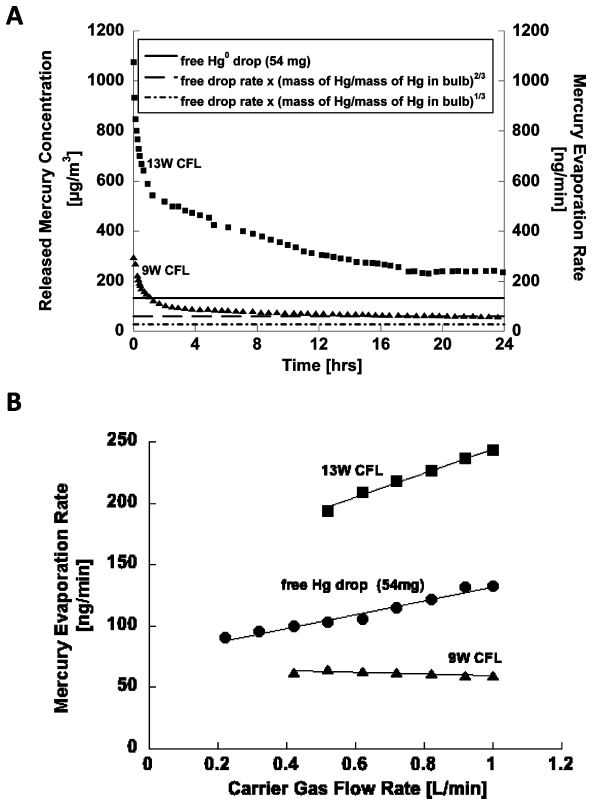

FIGURE 1. Mercury vapor release characteristics for two brands of compact fluorescent lamps following catastrophic fracture at room temperature. A: Hg-vapor concentrations and release rates in a 2 L PTFE enclosure purged with a 1 L/min flow. For comparison, the plot shows the evaporation rate from a free Hg° drop corrected for differences in the Hg mass between the drop and the bulb for two limiting cases: convective mass transfer at constant mass transfer coefficient (rate ≈ area ≈ mass$^{2/3}$) and diffusion dominated mass transfer from a drop (rate ≈ K × area ≈ mass$^{1/3}$). B: Mercury evaporation rate as a function of gas flow rate over the broken lamp showing a weak influence of convection.

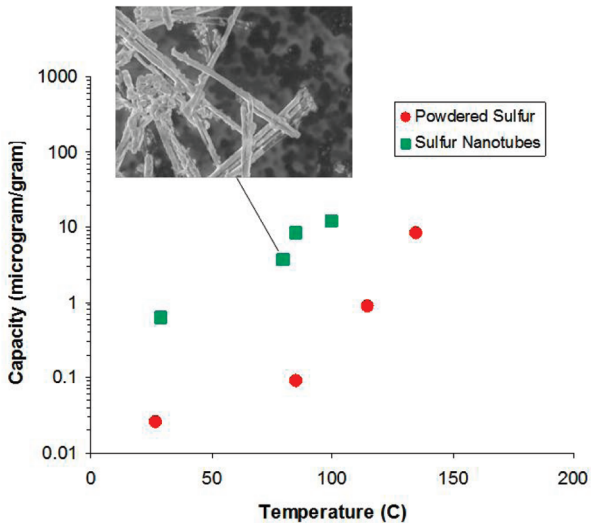

FIGURE 2. Standard Hg adsorption capacities for elemental sulfur nanotubes and conventional sulfur powder as a function of adsorption reaction temperature. Image is SEM micrograph of template S-nanotubes.

nanoparticles as room-temperature Hg sorbents and compare them to conventional microscale powders. Table 1 shows that mercury capacities vary greatly with chemistry (Ag > Cu > Ni > Zn) and, for each metal, are significantly enhanced by nanosynthesis. The rank order parallels the standard free energies for metal oxidation, $nM + {}^1/_2O_2 \rightarrow M_nO_2$ (Ag_2O, $\Delta G_f^\circ = -9.3$ kJ/mol; CuO, $\Delta G_f^\circ = -133.5$ kJ/mol; NiO, $\Delta G_f^\circ = -216$ kJ/mol; ZnO, $\Delta G_f^\circ = -318.5$ kJ/mol), and (complete) oxidation of copper is shown to greatly reduce its sorption activity (31.8 to 4.3 μg/g). Interestingly, copper metal activity is observed to increase modestly as the fresh metal nanoparticles age in the atmosphere, which may suggest elevated activity for *partially* oxidized surfaces. The nanometal capacities represent from about 10^{-6} (Zn) to 35% (Ag) of theoretical monolayer coverage on the nominal outer surfaces indicating that the process is far from reaching stoichiometric alloy formation, even in an outer shell, and the reactions are limited to specific active surface sites under these low temperature conditions. Among these metal sorbents, nanosilver is potentially attractive as a high-capacity sorbent (capacities up to 8510 μg/g) for room temperature applications like CFL capture. Annealing nano-silver reduces both its surface area and Hg capture capacity (Table 1).

Granite et al. (*28*) investigated metal sulfides MoS_2 and FeS_2 as Hg sorbents at elevated temperature and report a high capacity for MoS_2. In preliminary experiments, we found WS_2 to be significantly more reactive than MoS_2 (both conventional powders) and therefore were motivated to test WS_2 nanoparticles as potential high-capacity sorbents. In this case, nanosynthesis offered no significant advantage, and none of the metal sulfides appear among the most active and useful low-temperature sorbents in Table 1.

Carbon Materials. Activated carbons are widely used to capture mercury vapor, and their performance can be enhanced by surface modification with sulfur, halogen, or oxygen-containing functional groups (*18, 28–33*). Because carbons are capable of developing extensive *internal* surface area, there is little motivation to enhance the *external* surface area through nanosynthesis methods. Here we evaluate carbons as readily available reference materials that are market-relevant benchmarks for the new nanosorbents. Table 1 shows low to modest capacities on carbons (0.45−115 μg/g) with the exception of the S-impregnated material (2600 μg/g), which is one of best commercially available sorbents in this study.

Selenium-Based Materials. Selenium has an extremely high affinity for mercury. In the body, it sequesters mercury into insoluble and metabolically inactive mercury selenides and by this mechanism is protective against mercury neurotoxicity (*9, 34*). Its antioxidant nature helps to protect against mercury-induced DNA damage (*35*). In the environment the stable sequestration of mercury by selenium may reduce its mobility, bioavailability, and ecotoxicity (*9, 36, 37*). Strong Hg/Se binding may be key to understanding the biological and environmental behavior of both mercury and selenium (*38–40*). There are few published studies of selenium-based mercury vapor capture, although selenium has been used in Hg removal from off gases in sulfide ore processing (*41*) and is being considered for Hg stockpile stabilization and long-term storage (*42*). The presumed capture mechanism is reaction to HgSe ($\Delta G_f^\circ = -38.1$ kJ/mol) (*43*).

Here we focus on amorphous nanoselenium, which has received recent attention in chemoprevention (*17*) but has not to our knowledge been used for low-temperature Hg vapor capture. Figure 3 shows the colloidal synthesis of nanoselenium, the particle size distributions, and the mercury capture behavior of competing Se forms. The original synthesis method uses glutathione (GSH) as a reductant and bovine serum albumin (BSA) as a surface stabilizing agent to achieve very small particles in colloidal suspension (*17*) as shown in Figure 3A, left. Surprisingly the BSA-stabilized nano-Se has a lower capacity than conventional Se powder

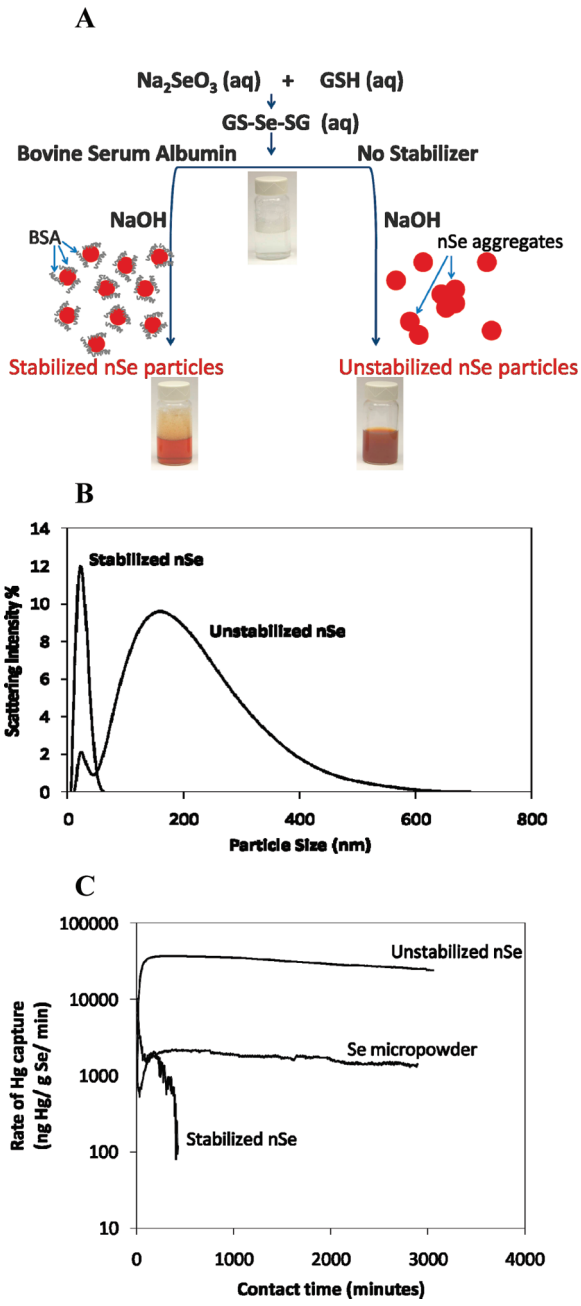

FIGURE 3. Synthesis, particle size distributions, and Hg-uptake kinetics of competing forms of selenium. A: Colloidal synthesis of BSA-stabilized (left) and unstabilized (right) nano-Se. B: Particle-size distributions in aqueous media by dynamic light scattering (*44*). C: Hg-uptake kinetics under standard conditions (60 μg/m^3).

despite the *much* smaller particle size (6−60 nm vs 10−200 μm). We hypothesized that the protein stabilizer (BSA) either blocked Hg access to the Se surfaces or chemically passivated the surfaces through Se−thiol interactions. We therefore removed the BSA, as shown in Figure 3A, right, to make "unstabilized nano-Se", which Figure 3C shows to have a remarkably high Hg sorption capacity and much faster kinetics than conventional micro-Se. Mercury uptake continues over very long times, and a 184 h experiment was necessary to approach the end state, at which point the unstabilized nano-Se had adsorbed 188 000 μg Hg/g or approximately 20% Hg/Se mass ratio. X-ray diffraction analysis shows both the micro-Se and unstabilized nano-Se are amorphous, as is the stabilized nano-Se (*45*).

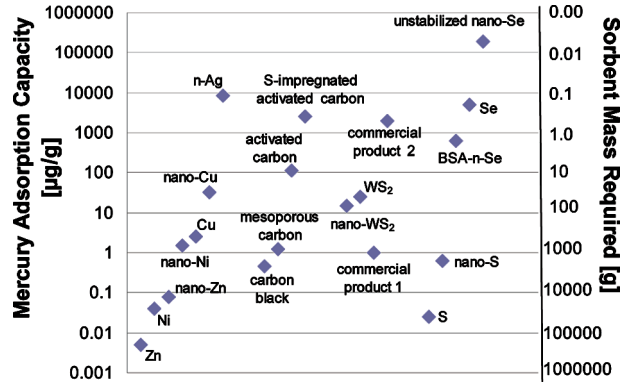

FIGURE 4. Comparison of the sorbents in this study. Left axis: Standard Hg adsorption capacity. Right axis: Amount of sorbent required for capture of 1 mg of Hg vapor typical of the total release from a single CFL over a three-day period.

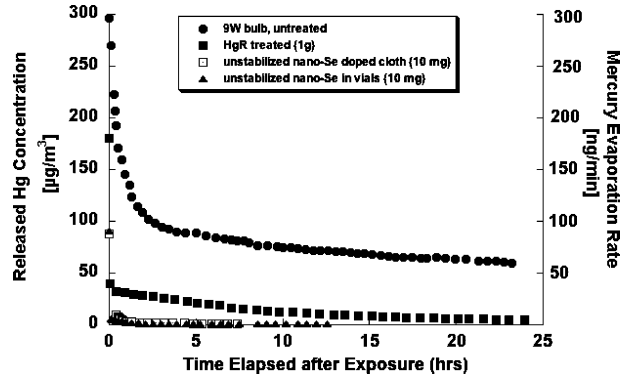

FIGURE 5. Effect of sorbents applied in situ on mercury vapor release following catastrophic fracture of a CFL at room temperature. Top curve: No sorbent. Bottom curves: Same CFL broken in presence of sulfur-impregnated activated carbon (1 g of HgR) and unstabilized nano-selenium (10 mg) either as dry nanopowder or impregnated cloth. The integrated mercury released over the course of this experiment is 113 (untreated lamp), 20 (1 g of HgR treatment), 1.6 (Se in vials), and 1.2 μg (Se-impregnated cloth).

Comparison of Sorbents. Figure 4 shows a comparison of the new and reference sorbents in this study. The right-hand axis gives the amount of sorbent required to capture 1 mg of Hg vapor, typical of CFL release. Surprisingly, some common sorbents such as powdered S or Zn require enormous amounts of material (>10 kg) to treat the vapor released from a single CFL and most of the sorbents require amounts that are not attractive for incorporation into consumer packaging (>10 g). A small number of sorbents (nano-Ag, S-impregnated activated carbon, and two selenium forms) have capacities that should allow <1 g of sorbent to be used. The most effective sorbent is unstabilized nano-Se, which can capture the contents of a CFL with amounts less than 10 mg. This capacity corresponds to about five monolayer equivalents indicating significant subsurface penetration of mercury into selenium nanoparticles (unlike the other sorbents). The capacity is still only about 7% of the bulk stoichiometric conversion to HgSe, however, indicating the potential for further capacity improvement by sorbent optimization.

In Situ Capture of CFL Mercury. Although the amount of Hg released from CFLs on fracture is small (typically <1 mg), only a few sorbents have sufficient capacity to sequester it all at room temperature for practical application (see Figure 5). For in situ capture, where the sorbent is supplied to consumers in the form of a safe disposal bag, impregnated cloth, or modified retail package, only nano-Ag, selenium

forms, or sulfur-impregnated activated carbon could be used in reasonable quantities. The concept of in situ capture is demonstrated below, here "treatment" is defined as sealing the fractured CFL and sorbent in a confined space for 24 h, then removing the sorbent and measuring the residual vapor release.

The commercial sulfur-impregnated activated carbon reduced the mercury release by 83% over the untreated bulb, making it a viable candidate for in situ capture of mercury vapor. Moreover, the low cost and low toxicity of this material make it an attractive option for consumer use. Even better performance was exhibited by the unstabilized nano-selenium, which decreased the mercury release by 99% over an untreated bulb, regardless of the application method, and with 100-fold less sorbent mass. Nearly complete suppression of mercury vapor from fractured lamps can be achieved by sealing the lamp in a confined space with 10 mg of unstabilized nano-selenium for 24 h, either as an impregnated cloth draped over the fractured bulb or as a loose powder in vials.

The present article provides sufficient motivation to pursue further development of sorbent-based technologies for suppressing mercury vapor release from broken fluorescent lamps. Work is underway to engineer (i) sorbent-impregnated reactive barrier cloths for remediation of porous substrates such as carpets at break sites and (ii) sorbent-containing disposal bags or recycle boxes to allow safe handling and stable disposition in the environment. Important issues in this development include reaction kinetics, landfill stability, impregnated cloth design, bag design, and management of secondary risks to both human health and the environment associated with possible release or and exposure to the nanomaterial sorbents themselves.

Acknowledgments

Financial support was provided by the NIEHS Superfund Basic Research Program P42 ES013660. While this work was supported financially by the NIEHS, the article does not necessarily reflect the views of the agency. The technical contributions of Chris Wang, Aihui Yan, and Professor Steven Hamburg from Brown University are gratefully acknowledged.

Supporting Information Available

Additional information on the methods, figures showing an example breakthrough curve for the fixed-bed sorbent experiments and SEM images of nano-silver particles before and after vacuum annealing, additional discussion, additional references. This material is available free of charge via the Internet at http://pubs.acs.org.

Literature Cited

(1) Jang, M.; Hong, S. M.; Park, J. K. Characterization and recovery of mercury from spent fluorescent lamps. *Waste Manage.* **2005**, *25*, 5–14.
(2) EPA Final Rule, Hazardous Waste Management System, Modification of the HazardousWaste Program, Hazardous Waste Lamps, Federal Register, 1999; Vol. 64, No. 128.
(3) Raposo, C.; Windmoller, C. C.; Junior, W. A. D. Mercury speciation in fluorescent lamps by hermal release analysis. *Waste Manage.* **2003**, *23*, 879–886.
(4) Baughman, T. A. Elemental mercury spills. *Environ. Health Perspect.* **2006**, *114* (2), 147–152.
(5) Thaler, E. G.; Wilson, R. H.; Doughty, D. A.; Beers, W. W. Measurement of mercury bound in the glass envelope during operation of fluorescent lamps. *J. Electrochem. Soc.* **1995**, *142* (6), 1968–1970.
(6) Tunnessen, W. W.; McMahon, K. J.; Baser, M. Acrodynia: Exposure to mercury from fluorescent light bulbs. *Pediatrics* **1987**, *79* (5), 786–789.
(7) Celo, V.; Lean, D. R. S.; Scott, S. L. Abiotic methylation of mercury in the aquatic environment. *Sci. Total Environ.* **2006**, *368*, 126–137.
(8) Gilbert, S. G.; Grant-Webster, K. S. Neurobehavioral effects of developmental methylmercury exposure. *Environ. Health Perspect.* **1995**, *103* (6), 135–142.
(9) Raymond, L. J.; Ralston, N. VC. Mercury: selenium interactions and health implications. *Seychelles Med. Dent. J.* **2004**, *7* (1), 72–77.
(10) Jones, R. L.; Sinks, T.; Schober, S. E.; Pickett, M. Blood mercury levels in young children and childbearing-aged women—United States, 1999−2002. *Morbidity and Mortality Weekly Rep.* **2004**, *53* (43), 1018–1020.
(11) Iyengar, G. V.; Rapp, A. S. O. Human placenta as a "Duel" biomarker for monitoring fetal and maternal environment with special reference to potentially toxic trace elements. Part 3: Toxic trace elements in placenta and placenta as a biomarker for these elements. *Sci. Total Environ.* **2001**, *280* (1−3), 221–238.
(12) Dang, T. A.; Frisk, T. A.; Grossman, M. W.; Peters, C. H. Identification of mercury reaction sites in fluorescent lamps. *J. Electrochem. Soc.* **1999**, *146* (10), 3896–3902.
(13) Johnson, M. L.; Lai, H. Y.; Wortman, D. Preventing mercury emissions from coal-fired plants using environmentally preferable coal purchasing practices. *J. Cleaner Prod.* **2008**, *16*, 716–721.
(14) Jian, K.; Truong, T. C.; Hoffman, W. P.; Hurt, R. H. Mesoporous carbons with self-assembled surfaces of defined crystal orientation. *Microporous Mesoporous Mater.* **2008**, *108* (1−3), 143–151.
(15) Painter, E. P. The chemistry and toxicity of selenium compounds, with special reference to the selenium problem. *Chem. Rev.* **1941**, *28* (2), 179–213.
(16) Ganther, H. E. Selenotrisulfides. Formation by the reaction of thiols with selenious acid. *Biochemistry* **1968**, *7* (8), 2898–2905.
(17) Zhang, J. S.; Gao, X. Y.; Zhang, L. D.; Bao, Y. P. Biological effects of nano red elemental selenium. *Biofactors* **2001**, *15* (1), 27–38.
(18) Manchester, S.; Wang, X.; Kulaots, I.; Gao, Y.; Hurt, R. High capacity mercury adsorption on freshly ozone-treated carbon surfaces. *Carbon* **2008**, *4* (3), 518–524.
(19) Fuhrmann, M.; Melamed, D.; Kalb, P. D.; Adams, J. W.; Milian, L. W. Sulfur polymer solidification/stabilization of elemental mercury waste. *Waste Manage.* **2002**, *22*, 327–333.
(20) Oji, L. N. Mercury disposal via sulfur reactions. *J. Environ. Eng.* **1998**, *124* (10), 945–952.
(21) Svensson, M.; Allard, B.; Duker, A. Formation of HgS-mixing HgO or elemental Hg with S, FeS, or FeS_2. *Sci. Total Environ.* **2006**, *368*, 418–423.
(22) Guo, Y.; Zhao, J.; Yang, S.; Yu, K.; Wang, Z.; Zhang, H. Preparation and characterization of monoclinic sulfur nanoparticles by water-in-oil microemulsions technique. *Powder Technol.* **2006**, *162*, 83–86.
(23) Bezverkhyy, I.; Afanasiev, P.; Marhic, C.; Danot, M. Template-free solution synthesis of sulphur microtubules. *Chem. Mater.* **2003**, *15*, 2119–2121.
(24) Hrbek, J.; Li, S. Y.; Rodriguez, J. A.; Campen, D. G.; Huang, H. H.; Xu, G. Q. Synthesis of sulfur films from S_2 gas: Spectroscopic evidence for the formation of S_n species. *Chem. Phys. Lett.* **1997**, *267*, 65–71.
(25) Poulston, S.; Granite, E. J.; Pennline, H. W.; Myers, C. R.; Stanko, D. P.; Hamilton, H.; Rowsell, L.; Smith, W. J.; Ilkenhans, T.; Chu, W. Metal sorbents for high temperature mercury capture from flue gas. *Fuel* **2007**, *86*, 2201–2203.
(26) Yan, T. Y. A novel process for Hg removal from gases. *Ind. Eng. Chem. Res.* **1994**, *33*, 3010–3014.
(27) Levlin, M.; Ikävalko, E.; Laitinen, T. Adsorption of mercury on gold and silver surfaces. *Fresenius' J. Anal. Chem.* **1999**, *365*, 577–586.
(28) Granite, E. J.; Pennline, H. W.; Hargis, R. A. Novel sorbents for mercury removal from flue gas. *Ind. Eng. Chem. Res.* **2000**, *39*, 1020–1029.
(29) Hsi, H.; Rood, M. J.; Rostam-Abadi, M.; Chen, S.; Chang, R. Effects of sulfur impregnation temperature on the properties and mercury adsorption capacities of activated carbon fibers (ACFs). *Environ. Sci. Technol.* **2001**, *35*, 2785–2791.
(30) Korpiel, J. A.; Vidic, R. D. Effect of sulfur impregnation method on activated carbon uptake of gas-phase mercury. *Environ. Sci. Technol.* **1997**, *31*, 2319–2325.
(31) Li, Y. H.; Lee, C. W.; Gullett, B. K. Importance of activated carbon's oxygen surface functional groups on elemental mercury adsorption. *Fuel* **2003**, *82* (4), 451–457.
(32) Olson, E. S.; Miller, S. J.; Shara, R. K.; Dunham, G. E.; Benson, S. A. Catalytic effects of carbon sorbents for mercury capture. *J. Haz. Mater.* **2000**, *74* (1−2), 61–79.
(33) Ghorishi, S. B.; Keeney, R. M.; Serre, S. D.; Gullett, B. K.; Wojciech, S.; Jozewicz, S. Development of a Cl-impregnated activated

carbon on entrained-flow capture of elemental mercury. *Environ. Sci. Technol.* **2002**, *36*, 4454–4459.
(34) Newland, M. C.; Reed, M. N.; LeBlanc, A.; Donlin, W. D. Brain and blood mercury and selenium after chronic developmental exposure to methylmercury. *Neurotoxicology* **2006**, *27*, 710–720.
(35) Tran, D.; Moody, A. J.; Fisher, A. S.; Foulkes, M. E.; Jha, A. N. Protective effects of selenium on mercury-induced DNA damage in mussel haemocytes. *Aquatic Toxicology* **2007**, *84*, 11–18.
(36) Falnoga, I.; Tusek-Znidaric, M. Selenium-mercury interactions in man and animals. *Biol. Trace Elem. Res.* **2007**, *119*, 212–220.
(37) Cabanero, A. I.; Madrid, Y.; Camara, C. Mercury-selenium species ration in representative fish samples and their bioaccessibility by an in-vitro digestion method. *Biol. Trace Elem. Res.* **2007**, *119* (3), 195–211.
(38) Bates, C. J.; Prentice, A.; Birch, M. C.; Delves, H. T.; Sinclair, K. A. Blood indices of selenium and mercury, and their correlations with fish intake, in young people living in Britain. *Br. J. Nutr.* **2006**, *96*, 523–531.
(39) Ralston, N. VC.; Blackwell III, J. L.; Raymond, L. J. Importance of molar ratios in selenium-dependent protection against methylmercury toxicity. *Biol. Trace Elem. Res.* **2007**, *119* (3), 255–268.
(40) Chen, C.; Yu, H. Zhao, J.; Li, B.; Qu, L.; Liu, S.; Zhang, P.; Chai, Z. The roles of serum selenium and selenoproteins on mercury toxicity in environmental and occupational exposure. *Environ. Health Perspect.* **2006**, *114* (2), 297–301.
(41) Habashi, F. Metallurgical plants: How mercury pollution is abated. *Environ. Sci. Technol.* **1978**, *12* (13), 1372–1376.
(42) Randall, P.; Brown, L.; Deschaine, L.; Dimarzio, J.; Kaiser, G.; Vierow, J. Application of the analytic hierarchy process to compare alternatives for the long-term management of surplus mercury. *J. Environ. Manag.* **2004**, *71*, 35–43.
(43) Ratajczak, E.; Terilowski, J. Thermodynamic Properties of Mercury Selenide. *Akad. Med. Wrokleuv Pol. Rocziniki Chem.* **1968**, *42* (3), 433–436.
(44) Murdock, C. R.; Braydish-Stolle, L.; Schrand, M. A.; Schlager, J. J.; Hussain, M. S. Characterization of nanomaterial dispersion in solution prior to in vitro exposure using dynamic light scattering technique. *Toxicol. Sci.* **2008**, *101* (2), 239–253.
(45) Bagnall, K. W. *The Chemistry of Selenium, Tellurium and Polonium*; Elsevier Publishing Company: Dordrecht, The Netherlands, 1966; p 34

ES8004392